Biochimica et Biophysica Acta 1797 (2010) 347–359

Contents lists available at ScienceDirect

Biochimica et Biophysica Acta

journal homepage: www.elsevier.com/locate/bbabio

Redox potential of the Rieske iron–sulfur protein Quantum-chemical and electrostatic study

Andrey M. Kuznetsov [a,*], Ekaterina M. Zueva [a], Alexei N. Masliy [a], Lev I. Krishtalik [b,*]

[a] Kazan State Technological University, ul. K. Marksa 68, 420015, Kazan, Russia
[b] Frumkin Institute of Physical Chemistry and Electrochemistry, Russian Academy of Sciences, Leninskii pr. 31, 119991 Moscow, Russia

ARTICLE INFO

Article history:
Received 27 July 2009
Received in revised form 4 December 2009
Accepted 8 December 2009
Available online 21 December 2009

Keywords:
Rieske protein
Redox potential
Protein's dielectric permittivity
Density functional calculation
Broken symmetry approach
Absolute electrode potential

ABSTRACT

Quantum-chemical study of structures, energies, and effective partial charge distribution for several models of the Rieske protein redox center is performed in terms of the B3LYP density functional method in combination with the broken symmetry approach using three different atomic basis sets. The structure of the redox complex optimized in vacuum differs markedly from that inside the protein. This means that the protein matrix imposes some stress on the active site resulting in distortion of its structure. The redox potentials calculated for the real active site structure are in a substantially better agreement with the experiment than those calculated for the idealized structure. This shows an important role of the active site distortion in tuning its redox potential. The reference absolute electrode potential of the standard hydrogen electrode is used that accounts for the correction caused by the water surface potential. Electrostatic calculations are performed in the framework of the polarizable solute model. Two dielectric permittivities of the protein are employed: the optical permittivity for calculation of the intraprotein electric field, and the static permittivity for calculation of the dielectric response energy. Only this approach results in a reasonable agreement of the calculated and experimental redox potentials.

1. Introduction

Iron–sulfur proteins (ISP) present an important class of redox proteins having widely varying properties. Among them, the Rieske ISP posseses one of the most positive redox potentials. This protein is an ubiquituos component of the electron transport chain of cytochrome bc_1 or b_6f complexes; it is present also in some other systems, e.g. dioxigenases and arsenite oxidase. In cytochrome bc_1 or b_6f complexes, its physiological function is to accept one reducing equivalent (electron and proton) from quinol and to transfer it to *cyt* c_1 or *cyt f* (for review see e.g. [1–5]). The Rieske protein consists of two parts: the intramembrane domain anchoring the protein to the proper place, and the extrinsing head containing the redox center. The extrinsing head performs a hinge movement contacting in turn the quinol binding site and the corresponding cytochrome, this movement being a part of the total electron transfer process.

The active site of the Rieske protein presents an iron–sulfur cluster [2Fe2S] with one Fe atom liganded by two His, and the other by two Cys. The presence of His ligands distinguishes the Rieske protein from other ISP's. The formal oxidation state of iron atoms in reduced state is $Fe^{II}Fe^{III}$, in oxidized state—$Fe^{III}Fe^{III}$.

The extrinsic head can be cleaved out of the whole complex, and this allows the study of its structure by X-ray crystallography [6,7]. Recently, a detailed high resolution study of the structure of the wild type protein from *Rhodobacter sphaeroides* and its several mutants has been published [8]. We will use these data in our subsequent calculations.

While several papers are dealing with theoretical calculations of the ISP redox potentials [9–20], only one of them considers the Rieske protein [15] (in this paper as well as in [21] also the values of p*K*'s were calculated).[1] In all these papers quantum-chemical analysis is combined with calculations of the electrostatic energy. This combination proceeds in two modes. The first one can be called a full or total calculation. It does not resort to any experimentally determined redox potential but uses the energies calculated quantum-chemically and the electrostatic energies calculated using the atomic partial charges

Abbreviations: B3LYP, gradient-corrected functional described by a combination of Becke's three parameter (B3) hybrid exchange functional and the Lee–Yang–Parr (LYP) correlation functional; BS, broken symmetry approach; CD, circular dichroism; DFT, density functional theory; ESP charges, atomic charges fitted from the molecular electrostatic potential; ExtC, extended model complex; *emf*, electromotive force; ISP, iron–sulfur protein; MinC, minimal model complex; pdb, Protein Data Bank identifier; SCF, self-consistent field; S.H.E., standard hydrogen electrode; 6-31G(d,p), standard split-valence atomic basis set including polarization functions on all the atoms; 6-31++G(d,p), the same supplemented by diffuse Gaussian components on all the atoms; TZVP, triple-zeta split-valence basis set supplemented by polarization functions; UB3LYP, spin-unrestricted version of B3LYP; WT, wild type

* Corresponding authors.
E-mail addresses: am_kuznetsov@kstu.ru (A.M. Kuznetsov), av164159@comtv.ru (L.I. Krishtalik).

[1] The quantum chemical analysis of the Rieske protein active center has been performed also in [22–24]. Calculation of its redox potential was not the task of these papers.

0005-2728/$ – see front matter © 2009 Elsevier B.V. All rights reserved.
doi:10.1016/j.bbabio.2009.12.004

found from quantum chemistry [13–16]. The other approach is to compute the electrostatic transfer energy of the redox center into the corresponding protein from some solvent for which the redox potential is known experimentally. In this case, the quantum-chemical partial atomic charges fitted to reproduce the electrostatic potential around the molecule (so-called electrostatic potential charges, ESP charges) are employed.

The specific feature of the iron–sulfur clusters comprising two or more Fe atoms is the coupling of their spins. The correct quantum-chemical treatment of such systems can be achieved within the broken symmetry (BS) approach developed by Noodleman et al. [13–16,25–30] (for details see Section 2). For iron–sulfur clusters, the most detailed calculations in the framework of the BS approach were done by Noodleman et al. [13–16]. The partial charges obtained in these studies were used also in the transfer energy calculations in [17–20].

In the present study, we will reconsider the redox potential of the Rieske protein. Our approach differs from that of [15] in some aspects. First, we modify the calculation of the redox potential basing on our analysis of the absolute electrode potential given recently [31]. Second, we will take into account the presence of two physically different components of the electrostatic energy, viz. the dielectric response energy and the energy of charges in the intraprotein electric field; the semi-continuum calculation of these two components demands for employment of two dielectric permittivities—the static and the optical ones [32]. The last approach has been used successfully in [20,33]. A more detailed description of these problems is done below, in Section 3.

2. Computational methods

2.1. Quantum-chemical calculations

2.1.1. Methods

Quantum-chemical calculations were carried out using the GAUSSIAN 03 program package [34] and employing the density functional theory (DFT). The latter uses the B3LYP gradient-corrected functional described by a combination of Becke's three parameter (B3) hybryd exchange functional [35] and the Lee–Yang–Parr (LYP) correlational functional [36]. All calculations of complexes with unpaired electrons (open-shell systems) were done using the spin-unrestricted formalism (UB3LYP). Full or partial geometry optimizations were carried out with the standard 6-31G(d,p) basis set. For fully optimized complexes, the geometry optimization was followed by analytical second-derivative calculations to ensure that the optimized structures correspond to minima on the potential energy surfaces (no imaginary frequences). The same calculations allowed the estimation of the thermal and vibrational corrections to the gas phase Gibbs free energies. These corrections were calculated for 298.15 K and 1 atm. For comparison, we used also the contracted TZVP basis set reported by Ahlrichs et al. [37,38]. This all-electron basis set is commonly applied in the framework of the UB3LYP-BS (for BS see bellow) computational procedure [39–41].

It is well known, that in energy calculations for radicals, anions and systems with significant negative charges or systems with low ionization potentials, the employment of basis sets suplemented by diffuse functions is strongly recommended. On this reason, in our calculations of energies we used additionally the 6-31++G(d,p) basis set which includes diffuse components of Gaussian functions on all the atoms including hydrogens.

In the cases of TZVP and 6-31++G(d,p) basis sets, to obtain the gas phase Gibbs free energies of complexes under study we used the zero-point energies (ZPE) and thermal corrections obtained at the B3LYP/6-31G(d,p) level. In other words, these corrections were added to the ground state total energies obtained with TZVP and 6-31++G(d,p) basis sets from single-point SCF calculations using the tight SCF convergence criterion at the B3LYP/6-31G(d,p) optimized geometries (for details, see Section 3.1.3).

2.1.2. Spin coupling effects

In calculations for the binuclear complexes with [2Fe2S] cores, the effects of spin coupling between unpaired electrons of the two iron centers must be taken into account, as well as the resonance delocalization effects (if one considers a mixed-valence dimer). In the oxidized $Fe^{III}Fe^{III}$ form, both iron centers are described by the spin quantum numbers S_1 and S_2 with the same value of 5/2. The pure spin energies of an iron dimer can be described by the following spin Hamiltonian:

$$\widehat{H} = -2J_{ox}\widehat{S}_1\cdot\widehat{S}_2. \tag{1a}$$

The reduced $Fe^{II}Fe^{III}$ form comprises a mixed-valence cluster with spins $S_1 = 2$ and $S_2 = 5/2$. The additional electron can be delocalized over the Fe–Fe pair. The appropriate spin Hamiltonian modified by Shoji et al. [24] for unsymmetrical systems is given by

$$\widehat{H} = -2J_{red}\widehat{S}_1\cdot\widehat{S}_2 \pm \sqrt{\frac{\Delta^2}{4} + B^2\left(S+\frac{1}{2}\right)^2}. \tag{1b}$$

In formulas (1a and 1b), J_{ox} and J_{red} are the spin coupling parameters for the oxidized and reduced forms, B is the resonance delocalization parameter, S is the total spin quantum number with the permissible values lying in the range $|S_1 - S_2| \le S \le S_1 + S_2$, Δ is the potential energy difference (it equals to zero in case of an symmetrical system). Parameters of the above spin Hamiltonians have been estimated using the broken symmetry (BS) approach [13–15,25–30] according to formulas (2–5) as described in [24]:

$$J_{ox} = \frac{E_{BS} - E_{HS}}{\langle\widehat{S}^2\rangle_{HS} - \langle\widehat{S}^2\rangle_{BS}} \tag{2}$$

$$J_{red} = \frac{E_{BS1} - E^g_{HS} + \Delta E}{\langle\widehat{S}^2\rangle_{HS} - \langle\widehat{S}^2\rangle_{BS1}}, \quad \Delta E = \frac{|\Delta|}{2} - \sqrt{\frac{\Delta^2}{4} + 25B^2} \tag{3}$$

$$\Delta = E_{BS1} - E_{BS2} \tag{4}$$

$$B = \frac{\sqrt{(e^u_{HS} - e^g_{HS})^2 - \Delta^2}}{10}. \tag{5}$$

Herein, E_{HS} is the total energy of the high-spin (HS) state, E_{SB} is the total energy of a so-called BS state corresponding to a spin-unrestricted determinant in which the spin-up electrons are predominantly localized on one half of the binuclear cluster while the spin-down electrons—on the other half, ΔE is a correction term for the unsymmetrical double exchange interaction. For the reduced form, the computed HS state energy corresponds to the lowest HS state with delocalized spin-down d-electron in *gerade*-type orbital (E^g_{HS}). The resonance delocalization parameter B has been computed from the HS-state energy splitting between minority-spin orbitals corresponding to *ungerade* and *gerade* components of Fe(3d) orbitals in oxidized form. The energies of the pure low-spin states E^{ox}_S ($S = 0$) and E^{red}_S ($S = 1/2$, $S = 3/2$ or $S = 5/2$) for the oxidized and reduced forms are given by

$$E^{ox}_0 = E_{BS} + 5J_{ox} \tag{6}$$

$$E^{red}_{1/2} = E^g_{HS} + 24J_{red} + \sqrt{\frac{\Delta^2}{4} + 25B^2} - \sqrt{\frac{\Delta^2}{4} + B^2} \tag{7}$$

$$E^{red}_{3/2} = E^{g}_{HS} + 21J_{red} + \sqrt{\frac{\Delta^2}{4} + 25B^2} - \sqrt{\frac{\Delta^2}{4} + 4B^2} \quad (8)$$

$$E^{red}_{5/2} = E^{g}_{HS} + 16J_{red} + \sqrt{\frac{\Delta^2}{4} + 25B^2} - \sqrt{\frac{\Delta^2}{4} + 9B^2}. \quad (9)$$

2.1.3. Fitting of the ESP charges

The Merz–Singh–Kollman scheme [42,43] implemented in the GAUSSIAN program package was used to fit the point charges from the molecular electrostatic potential (ESP). As the van der Waals radii for H, C, N, O and S atoms the standard Merz–Kollman radii were employed: 1.2, 1.5, 1.5, 1.4 and 1.75 Å, respectively. For Fe atom in +2 and +3 oxidation states we used the same value of 1.4 Å. The values of radii 1.3 Å and 1.5 Å were also tested; the results were revealed to be weekly sensitive to this choice. No additional modifications to the charge fitting procedure were used in our calculations. The fitting Merz–Kollman (MK) charges were applied for subsequent electrostatic calculations.

Before the main electrostatic calculations, we performed the test calculations of the electric dipole moments of the imidazole and pyridine molecules using the 6-31G(d,p), TZVP and 6-31++G(d,p) basis sets. For imidazole, the obtained values are 3.703, 3.805 and 3.868 D for these three basis sets correspondingly, in comparison with experimental value of 3.67 D [44]. For pyridine, the corresponding values are in a similar sequence: 2.184, 2.299 and 2.378 D with the experimental value of 2.15 D [45]. As can be seen, the 6-31G(d,p) basis set gives a somewhat better agreement with experimental data. On this reason, for the subsequent electrostatic calculations we used as the main variant the charge distributions obtained within the 6-31G (d,p) basis set (for comparison, we tested also the other sets, but they give much worse results).

2.2. Electrostatic calculations

Semi-continuum electrostatic calculations were performed using the DelPhi software [46]. The atomic coordinates of the *R. sphaeroides* Rieske ISP wild type and Y156W mutant were taken from [8] (PDB entries 2NUK and 2NWF, correspondingly). Quantum-chemical analysis revealed some differences in structures of the reduced and oxidized active sites. However, no remarkable differences were observed by X-ray cristallography. In our calculations, we employed the experimental coordinates ascribing to each atom the partial charge obtained from quantum chemistry. In the model calculations of the redox center, the His, Cys, and Ser residues were replaced by imidazole, methylsulfide, and methanol molecules correspondingly; upon this modeling, the C–C bonds connecting these groups with the remaining part of the residue were scissed, and H atoms were added forming C–H bonds. The rest of each of these residues was accounted for in calculation of the intraprotein electric field. Due to an artificial inserting of H atoms, the distance between the remaining C and H becomes too short, and this should result in some overestimation of the positive potential set up by the residue. To avoid this error, the charge of the corresponding C atom was set to zero, and the emerging disbalance was distributed among the atoms connected with it. Without this redistribution, i.e. with the full partial charge on C, the energy of the redox center charges in the intraprotein electric field will be by ~0.05 eV higher; this shows that the possible error due to some arbitrarness in the new charge distribution is most probably substantially less than 0.05 eV.

The set of Konnoli's united atoms' radii usual for the DelPhi software was accepted, namely H 0.00 Å, C 1.90 Å, O 1.60 Å, N 1.65 Å, Cα 1.86 Å, S 1.90 Å, and Fe 0.70 Å. The Fe atoms are inaccessible to the external solvent, and therefore the value of their radius does not influence the van der Waals surface, and hence the electrostatic energy of the complex (tested by variation of this radius from 0.70 Å to 1.40 Å). In the calculations with the aqueous surroundings, the radius of the probe defining the solvent excluded surface was taken as 1.6 Å; we prefer this value as practically equal to the oxygen atom van der Waals radius.

The grid size employed for calculations of isolated complex was 131 (9.15 grid per Å), for the whole protein 181 (3.20 grid per Å). Variation of this parameter in limits of ±15% results in nonsystematic fluctuations in the effect of the intraprotein field in limits of 3 meV, and in the response energy in ±0.2 meV.

Calculations of the pre-existing intraprotein electric field were performed using the "optical" dielectric permittivity $\varepsilon_{o,p}$ reflecting the protein electronic polarizability [32]. The value of $\varepsilon_{o,p}=2.5$ was accepted corresponding to the usual refraction index of proteins close to 1.6. The value of $\varepsilon_{o,p}=2.5$ differs from the usual optical value for organic liquids (including amides) $\varepsilon_o \approx 2$. This is due to the higher protein's density (at the density ≈1.3 and the same polarizability of molecules or residues as in liquid, the Clausius–Mossotti equation gives $\varepsilon_{o,p} \approx 2.5$). On the contrary, for calculation of the dielectric response energy for a globule surrounded by an aqueous solution (in DelPhi software, this quantity is called the reaction field energy), the static dielectric permittivity of protein $\varepsilon_{s,p}$ (4 and higher) was used.

There are many different systems of partial charges. The AMBER 84 set is based on quantum-chemical calculations corrected in such a way to agree with the experimental dipole moments [47]. In other systems, e.g., AMBER 94 [48], the partial charges were empirically adjusted to describe the calculated energies, but they do not agree with the dipole moments. In our calculations (similar to those performed in [33]), we start with the AMBER 94 set; the partial charges of each neutral side chain (or dipolar component of partial charges of the charged side chains) and peptide group were scaled by the same factor to reproduce approximately the experimental dipole moment of the corresponding group. This reduced system, that is close to AMBER 84, was used as the starting point in calculations described below.

The quantum-chemical charge distribution was obtained by calculations in vacuum, i.e. the dielectric permittivity inside the molecule was equal by definition to 1. However, we consider protein as a system of partial charges imbedded in a medium with electronic polarizability ($\varepsilon_{o,p}=2.5$); this means that we fill with this medium the body of each aminoacid residue. This operation should decrease the field outside the group; therefore, to preserve the true original value of the external field we should increase the effective partial charges. Different scaling factors were used earlier [32,49–51] but the best substantiated from the physical point of view is that proposed by Mertz (personal communication). He pointed out that the field of a free charge placed in the center of a dielectric sphere does not change with the change of the intrasphere dielectric permittivity ε_i. However, when the spherical symmetry is broken, the external field can be described as a superposition of the fields of a free charge (if any) and some dipoles. The external field of the dipole component depends on the intra-body dielectric permittivity, namely, this field decreases as $3/(\varepsilon_i+2)$. Hence, to retain the original external field the partial charges corresponding to the dipole component should be multiplied by $(\varepsilon_{o,p}+2)/3$.[2] For the neutral residues, we employed their quantum-chemical partial charges modified by this factor (numerically, at $\varepsilon_{o,p}=2.5$, the scaling factor equals to 1.5, and it is close to that used in [32,49–51])[3]. For charged residues, their free partial charges were obtained as the difference of the corresponding partial

[2] Generally speaking, besides the dipole moment the higher moments (quadrupole, etc.) can be present. However, the scaling factors for these moments are close to that for dipole. The field of higher moments falls down with the distance faster than that of dipoles; hence, it plays a minor role. Therefore, in our study we restrict ourselves with the dipolar scaling factor.

[3] Another system of partial charges, viz. PARSE [52], gives dipole moments larger than those of free amides but similar to those that were evaluated from the experimental data for peptide group in proteins. The probable cause of the last effect is the electronic polarization of these groups inside the protein. Electrostatic calculations with PARSE charges and with those corrected as described above give rather similar results [20].

charges in the charged and neutral forms; these free charges remained uncorrected while for charges of the neutral form the correction described above is introduced. So, each of the partial charges of a charged residue presents a sum of the free (uncorrected) and dipolar (corrected) charges.

The Rieske protein ionizable groups are situated on the surface of the globule, and hence should have most probably p*K*'s similar to those in aqueous solutions. In our calculations, we accept that all these groups (except the neutral His 155) are in ionic state at pH ~ 7, and in alkaline solutions all lysines are neutral while arginines are neutral only in a strongly alkaline medium.

In a self-consistent quantum-chemical treatment of a solute combined with a continuum electrostatic description of the solvent effect, the quantum-chemical problem is to be solved taking into account explicitly the electric field set up on the molecule considered by its surroundings; in this scheme one does not need to introduce a specific intra-solute dielectric permittivity, it equals one by definition [53,54]. However, a much less laborious way is to use the molecule's model with characteristics obtained quantum-chemically for the molecule in vacuum, and to transfer it into a medium treated then electrostatically. In the last case, the most realistic model is the model of a polarizable solute, in particular with the optical intra-solute permittivity, that accounts for the solute's electronic polarization in the external field [53,54].

Taking into account that the active site of the Rieske ISP contains highly polarizable components (aromatic imidazoles and sulfur atoms) we accept its effective inner dielectric permittivity ε_i equal to 2.5. Ascribing to the solute the optical dielectric permittivity we need to correct its partial charges to preserve the value of the electric field outside the molecule. For this purpose, we use the following approximation. Similar to the method described above for the field of the protein dipoles, we increase the partial charges of a neutral protonated complex (in the $Fe^{III}Fe^{III}$ state) by a scaling factor $(\varepsilon_i + 2)/3$. The additional charges distributed over the complex upon its reduction (in sum −1) should not be corrected because they create the field of free charges, not of dipoles. For the sake of comparison, we will give below the results obtained both with these modified and uncorrected (vacuum) charges. Note that the account for the intra-solute dielectric permittivity affects only the energy of dielectric response because this quantity depends on the total charge of each atom; the solute energy in the external electric field (intraprotein field) is determined by the excess charges only, and hence does not depend on the correction described.

The dielectric response component was calculated in the following manner. First, the solute with the inner $\varepsilon_i = 2.5$ was transferred from the infinite medium of the same dielectric permittivity 2.5 into vacuum ($\varepsilon = 1$), and the energy of this transfer was calculated.[4] This energy was subtracted from the energy of transfer from medium of $\varepsilon_i = 2.5$ into protein. The last quantity was computed as a sum of two energies—the transfer energy into an infinite medium with a static dielectric permittivity of protein $\varepsilon_{s,p} = 4$ (or higher), and the response energy for protein with the inner constant $\varepsilon_{s,p}$ and an external dielectric permittivity of water $\varepsilon_{s,w} = 78$. This way was used in our previous works, e.g. [55–57], as well as by Zhou [58]. For systems of simple geometry like a spherical ion in a semi-infinite dielectric the analytical solution of the electrostatic problem gives the same result [59,60].

3. Results and discussion

3.1. Quantum-chemical calculations

The approach used in our work for calculation of redox potentials implies the choice of the model of the active site of the protein, i.e. the choice of atoms that are included in the quantum-chemical calculation scheme. The interaction of this active site with its protein environment is described within a continuum dielectric approach.

Our model is based on the experimental structure of the Rieske iron–sulfur protein [8]. The minimal complex (MinC) includes the [2Fe2S] core with two histidine ligands modeled by imidazole molecules (Im), and two cystein ligands modeled by methyl thiolate anions (CH_3S^-). The structure of this model complex $[Fe_2S_2(SCH_3)_2Im_2]$ is shown in Fig. 1. In the same figure, the structure of another model complex is also depicted. This extended complex (ExtC) includes additionally one methanol molecule (CH_3OH) bonded by a hydrogen bond to one of the sulfur atoms of [2Fe2S] core. In this case, the methanol molecule mimics the Ser 154 ligand in the Rieske protein structure.

One can assume, that the spatial positions of the frame atoms, namely, all heavy atoms of aminoacid residues ligating the iron–sulfur cluster are stabilized by the protein surroundings, and they depend weakly on the oxidation state of the complex. Experimentally, no difference in their coordinates in two oxidation states has been found [8]. Consequently, in the geometry optimization procedure of the model MinC and ExtC complexes the Cartesian coordinates of those atoms were fixed (these coordinates were taken from 2NUK.pdb structure [8]), and the coordinates of [2Fe2S] atoms as well as of all hydrogen atoms were fully optimized. The complexes optimized by such a way will be called in this paper the partly optimized complexes. Besides that, we have performed optimization of the MinC geometry with the optimization procedure extended to all its atoms. The total optimization was performed with the start geometry taken from the partly optimized MinC complexes. The obtained structure corresponds to the energy minimum on the total potential energy surface. In Fig. 2, we present for comparison the structure of this fully optimized MinC along with that of the partly optimized one.

For the ExtC complex, the geometry optimization was also performed for its mono- and bis-deprotonated forms. These deprotonated species were modeled by a successive removal of protons of His152 and His131 from the ExtC structure with the subsequent partial geometry optimization as described above.

3.1.1. Structures of the active site models

The typical shapes of the model complexes are depicted in Figs. 1 and 2, and the distances calculated are summarized in Table 1.

Calculations revealed a difference between coordinates in reduced and oxidized states: in the second case all distances between Fe atoms and their ligands are systematically shorter. Similar pecularities were observed in previous calculations on [2Fe2S] clusters [15,22–24]. That is the behavior one could expect. However, the experiment has not demonstrated such a difference. The reason for that is not quite clear. Maybe, as it is supposed in [8], this is due to reduction of the oxidized form upon exposure to high flux-X radiation. In any case, the experimental bond lengths of both Fe atoms with aminoacid ligands are practically equal to the arithmetic mean of two calculated values; so the agreement with the experiment is satisfactory. The same is true for the intracluster Fe–S bonds for one of Fe atoms but for the second Fe the experimental Fe–S bond length is markedly (by ~0.18 Å) shorter. The calculated length of the hydrogen bond S4-O1 for reduced ExtC is rather close to the experimental one. The data presented in Table 1 show that the Fe–Fe distance is shortened while going from the oxidized state to the reduced one. Similar results were obtained in [15,22,23] whereas Shoji et al. [24] found an opposite tendency.

The structures of partly and fully optimized minimal complexes (oxidation state $Fe^{II}Fe^{III}$) are compared at Fig. 2. The Fe-ligand bond lenghts in the fully optimized minimal complex and in the partly optimized complex differ not very strongly, in limits of ±0.02 Å; the difference in distances between nonbonded atoms inside the cluster is somewhat larger, up to 0.1 Å (Table 1). However, the mutual

[4] Note, that in calculation of the transfer energy from some solvent into protein (as was done in [20,33]) this step cancels out.

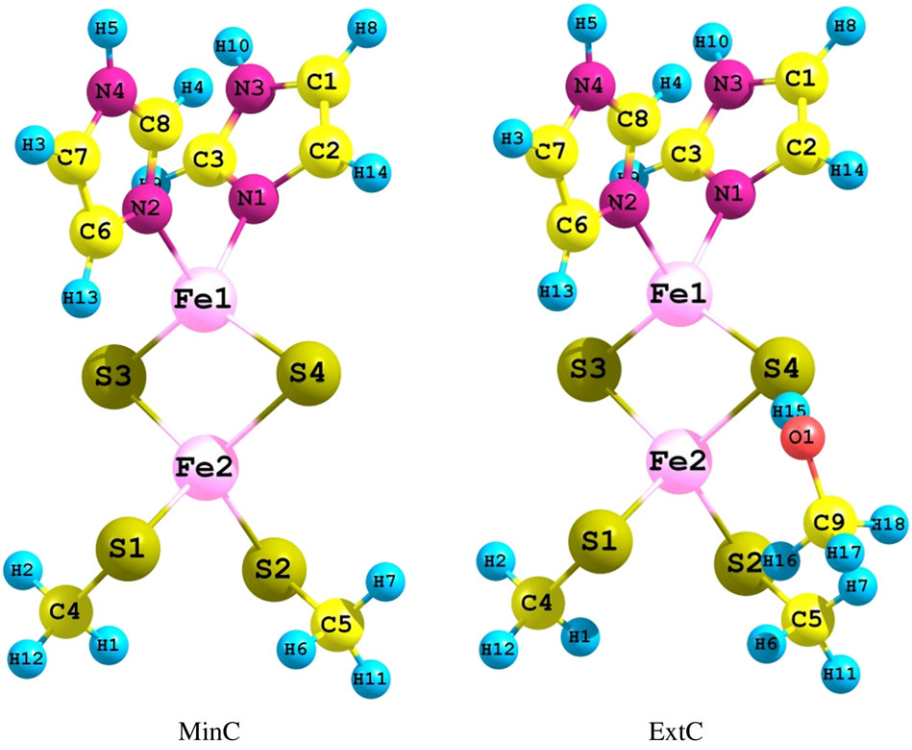

Fig. 1. Structures and atomic numbering of partly optimized minimal and extended model complexes ($Fe^{II}Fe^{III}$ oxidation state); the structures built using the ChemCraft visualization program [61] (see Table 1).

orientation of external ligands differs substantially from that in the experimental structure (upon the partial optimization, the coordinates of those ligands were fixed at their experimental values). So, the N1–N2 distance increased from 3.05 Å to 3.48 Å (oxidized form) or 3.62 Å (reduced form), the S1–S2 distance—from 3.70 Å to 3.87 Å or 3.84 Å, correspondingly. Both in the fully optimized and partly optimized complexes the plane of [2FeS2] core is somewhat distorted, the distortion for fully optimized complex is markedly stronger (Fig. 2). In the experimental structure, the situation is closer to the partly optimized complex. Such a change of the complex structure influences substantially its energy (see below, Section 3.2.2).

As can be seen from Table 1, in the course of deprotonation of the extended complex the Fe-ligand distances change not systematically.

3.1.2. Atomic charge distribution in the active site models

In Table 2 we collected the Mulliken and ESP atomic charges in minimal and extended complexes calculated quantum-chemically at the B3LYP level using the 6-31G(d,p) atomic basis set (see Subsection 2.1.3). As can be seen from these data, both the Mulliken and ESP charges on all S atoms are substantially more negative in the reduced state compared to the oxidized state. For N atoms, an opposite regularity is observed with Mulliken charges, with ESP charges of N1 the effect is variable.

For all the complexes in the oxidized state (and almost all in the reduced state), the effective Mulliken charge on Fe1 atom (which is liganded by histidines) is remarkably more positive compared to the Fe2 atom.

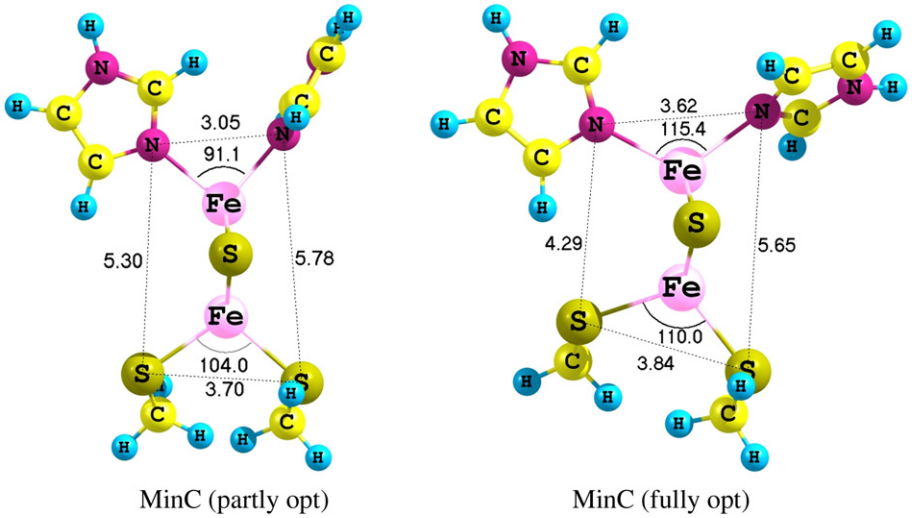

Fig. 2. Several interatomic distances (in Å) and bond angles (in degrees) in the partly and fully optimized minimal complexes for $Fe^{II}Fe^{III}$ oxidation state. In the orientation shown here one of the S atoms of [2Fe2S] core is hidden by another.

Table 1
Interatomic distances (Å) in redox center.

		Fe1–N1	Fe1–N2	Fe2–S1	Fe2–S2	Fe1–S3	Fe1–S4	Fe2–S3	Fe2–S4	Fe1–Fe2	S3–S4	S4–O1
Experiment: 2NUK.pdb		2.102	2.120	2.329	2.290	2.215	2.215	2.206	2.198	2.695	3.497	3.180
MinC, partly optimized	oxd	2.074	2.087	2.271	2.261	2.203	2.205	2.385	2.377	2.808	3.613	–
	red	2.129	2.140	2.352	2.338	2.230	2.231	2.390	2.373	2.599	3.794	–
MinC, fully optimized	oxd	2.101	2.103	2.283	2.267	2.219	2.211	2.386	2.368	2.905	3.518	–
	red	2.163	2.120	2.354	2.329	2.253	2.242	2.373	2.351	2.532	3.797	–
ExtC, partly optimized	oxd	2.071	2.082	2.272	2.259	2.202	2.209	2.381	2.384	2.817	3.607	3.315
	red	2.126	2.134	2.350	2.332	2.227	2.240	2.387	2.377	2.613	3.783	3.225
ExtC, 1-depr., partly optimized	oxd	1.975	2.107	2.285	2.281	2.237	2.248	2.343	2.346	2.847	3.594	3.244
	red	2.046	2.167	2.359	2.357	2.255	2.264	2.343	2.352	2.627	3.781	3.125
ExtC, 2-depr., partly optimized	oxd	1.996	2.001	2.312	2.304	2.284	2.297	2.309	2.314	2.863	3.592	3.232
	red	2.068	2.062	2.384	2.388	2.302	2.326	2.315	2.318	2.627	3.795	3.152

Atomic numbering according to 2NUK.pdb: Fe1: FE2 FES 200; Fe2: FE1 FES 200; N1: ND1 HIS 152; N2: ND1 HIS 131; S1: SG CYS 129; S2: SG CYS 149; S3: S2 FES 200; S4: S1 FES 200; O1: OG S154.

The distribution of ESP charges has a different character. For the oxidized form, in all the complexes under consideration the most positive Merz–Kollman charge is observed for the Fe2 atom. From our viewpoint, the ESP charges are rather conditional ones because they are used only for fitting the molecular electrostatic potential, and they do not have such a clear physical meaning as the Mulliken charges do. Therefore, they can hardly be considered as reflecting the real electron density distribution.

While going from the oxidized form to the reduced one the positive charge (both the Mulliken and ESP charge) on the Fe2 atom increases while on the Fe1 decreases (the only exception presents the fully optimized minimal complex). This at first glance unexpected positive shift of Fe2 charge upon reduction is compensated for by a remarkable negative shift of the charges on all sulfur atoms. Similar regularities were recently noted in [13] for other iron–sulfur clusters.

As for the deprotonated extended complexes, one can see that the positive values both of the Mulliken and ESP charges on Fe1 and Fe2 atoms increase on the whole while going from the protonated form to the bis-deprotonated one despite the total charge of the complex becoming more negative. Here we observe again the negative charge redistribution in favor of sulfur atoms.

It should be noted that the analysis of Mulliken and ESP charges calculated with TZVP as well as 6-31++G(d,p) basis sets demonstrated qualitatively the same regularities.

Table 2
Mulliken and ESP atomic charges in minimal and extended complexes calculated at the B3LYP/6-31G(d,p) level.

MinC (partly optimized)								
	Fe1	Fe2	N1	N2	S1	S2	S3	S4
oxd	0.862	0.561	−0.587	−0.594	−0.280	−0.262	−0.612	−0.596
	0.361	0.899	−0.128	−0.104	−0.501	−0.535	−0.588	−0.573
red	0.583	0.618	−0.528	−0.544	−0.370	−0.349	−0.767	−0.751
	0.253	1.012	−0.159	−0.057	−0.641	−0.644	−0.797	−0.780
MinC (fully optimized)								
	Fe1	Fe2	N1	N2	S1	S2	S3	S4
oxd	0.863	0.625	−0.595	−0.586	−0.320	−0.278	−0.639	−0.577
	0.522	0.977	0.027	−0.176	−0.502	−0.572	−0.683	−0.634
red	0.678	0.528	−0.528	−0.541	−0.398	−0.353	−0.779	−0.722
	0.256	0.971	−0.006	−0.043	−0.642	−0.630	−0.793	−0.768
ExtC (partly optimized)								
	Fe1	Fe2	N1	N2	S1	S2	S3	S4
oxd	0.895	0.566	−0.590	−0.600	−0.274	−0.252	−0.604	−0.668
	0.218	0.867	−0.015	0.005	−0.433	−0.504	−0.563	−0.561
red	0.631	0.622	−0.531	−0.552	−0.363	−0.335	−0.757	−0.814
	0.107	1.022	0.029	0.023	−0.570	−0.640	−0.780	−0.778
ExtC, mono-deprotonated (partly optimized)								
	Fe1	Fe2	N1	N2	S1	S2	S3	S4
oxd	0.945	0.558	−0.628	−0.587	−0.315	−0.293	−0.633	−0.718
	0.339	0.945	−0.043	0.006	−0.524	−0.575	−0.634	−0.625
red	0.706	0.582	−0.580	−0.534	−0.390	−0.379	−0.768	−0.841
	0.186	1.017	−0.029	0.076	−0.631	−0.701	−0.810	−0.792
ExtC, bis-deprotonated (partly optimized)								
	Fe1	Fe2	N1	N2	S1	S2	S3	S4
oxd	0.979	0.578	−0.616	−0.631	−0.344	−0.337	−0.670	−0.758
	0.465	0.991	−0.182	0.045	−0.570	−0.634	−0.707	−0.684
red	0.758	0.582	−0.566	−0.592	−0.416	−0.411	−0.792	−0.866
	0.436	1.071	−0.207	−0.034	−0.679	−0.744	−0.893	−0.861

Atomic numbering according to Fig. 1; Mulliken charges—first line, ESP (Merz–Kollman) charges—second line.

3.1.3. The gas phase energies of the active site models

In Table 3 we collected all energetics data needed for our subsequent calculations of redox potentials.

As can be seen from the data in Table 3, the ground state of all the complexes has a total spin $S=0$ and $S=1/2$ (except for bis-deprotonated complex) for oxidized and reduced forms, correspondingly. The negative values of exchange parameters J demonstrate an antiferromagnetic character of coupling between the two Fe centers. The parameters J can be compared directly with the experimental data. Their values for the exchange interaction between Fe(III) spin sites agree good enough with available experimental data for some similar systems: for spinach ferredoxin $J_{ox}=-183\ cm^{-1}$ [62], for synthetic analogue of oxidized 2Fe–2S proteins $J_{ox}=-149\ cm^{-1}$ [63], for *Synechococcus lividus* $J_{ox}=-185\ cm^{-1}$ [64], and for blue-green algae *Spirulina maxima* $J_{ox}=-182\pm20\ cm^{-1}$ [65]. For reduced complexes, the calculated exchange parameters are remarkably overestimated compared to the experimental value $J_{red}=-98+5/-10\ cm^{-1}$ for *S. maxima* [65].

The gas phase ionization free energies ΔG^{gas}_{red} were obtained as differences in total Gibbs free energies G^0_{298} of oxidized and reduced forms at 298.15 K. The values of G^0_{298} can be calculated by the following formula:

$$G^0_{298} = E_{elec}(0K) + ZPE + \delta G(0\rightarrow 298K),$$

where $E_{elec}(0\ K)$ is the total electronic energy at 0 K, ZPE is the zero-point energy, and the last item describes the thermal correction to the Gibbs free energy upon transition from 0 to 298 K.

As $E_{elec}(0\ K)$ we used the total electronic energies E_{GS} which were calculated for the ground states of complexes in the framework of the BS approach (see Table 3). Unfortunately, in the absence of the full structure optimization (restrictions imposed by the protein matrix) it is impossible to calculate reliably frequencies of all vibrations. Therefore, we used the ZPE and thermal corrections calculated from the thermochemical analysis of the fully optimized structures of the protonated as well as the mono- and bis-deprotonated complexes.

Table 3
Spin Hamiltonian parameters, ground state energies, gas phase ionization potentials and ionization Gibbs free energies calculated at the B3LYP level using three atomic basis sets.

		B (cm^{-1})	Δ (cm^{-1})	J (cm^{-1})	E_{GS} (Hartree)	IP^{gas}_{red} (eV)	ΔG^{gas}_{red} (eV)
MinC (partly optimized)							
$Fe^{III}Fe^{III}$	A			−163	−4652.45461		
($S=0$)	B			−168	−4653.03049		
	C			−171	−4652.53959		
$Fe^{II}Fe^{III}$	A	913	−7406	−280	−4652.51330	1.597	1.620
($S=1/2$)	B	1111	−6160	−313	−4653.09521	1.761	1.784
	C	1104	−5829	−317	−4652.60751	1.848	1.871
MinC (fully optimized)							
$Fe^{III}Fe^{III}$	A			−126	−4652.46445		
($S=0$)	B			−131	−4653.04016		
	C			−133	−4652.54981		
$Fe^{II}Fe^{III}$	A	1253	−6424	−285	−4652.52540	1.658	1.681
($S=1/2$)	B	1307	−5430	−289	−4653.10594	1.790	1.813
	C	1292	−5177	−291	−4652.61854	1.870	1.893
ExtC (partly optimized)							
$Fe^{III}Fe^{III}$	A			−157	−4768.18564		
($S=0$)	B			−162	−4768.80686		
	C			−165	−4768.27932		
$Fe^{II}Fe^{III}$	A	933	−7411	−276	−4768.25306	1.835	1.858
($S=1/2$)	B	1095	−6236	−304	−4768.88110	2.020	2.043
	C	1101	−5919	−310	−4768.35619	2.092	2.115
ExtC, mono-deprotonated (partly optimized)							
$Fe^{III}Fe^{III}$	A			−160	−4767.67312		
($S=0$)	B			−173	−4768.30002		
	C			−170	−4767.77455		
$Fe^{II}Fe^{III}$	A	942	−3902	−235	−4767.62685	−1.259	−1.217
($S=1/2$)	B	1007	−3071	−246	−4768.26528	−0.945	−0.903
	C	989	−2797	−245	−4767.74394	−0.833	−0.791
ExtC, bis-deprotonated (partly optimized)							
$Fe^{III}Fe^{III}$	A			−150	−4767.05399		
($S=0$)	B			−161	−4767.68888		
	C			−164	−4767.16658		
$Fe^{II}Fe^{III}$	A	1014	−1383	−201	−4766.90075	−4.170	−4.097
($S=3/2$)	B	1084	−1039	−218	−4767.55258	−3.709	−3.636
	C	1056	−817	−216	−4767.03675	−3.533	−3.460

1 Hartree = 27.2116 eV; A—6-31G(d,p), B—TZVP and C—6-31++G(d,p) atomic basis sets; S—total spin of the complex in the ground state (GS). The ionization Gibbs free energies were obtained as described in Section 2.1.1.

The quantum-chemical analysis allows us to find another important parameter—the inner-sphere reorganization energy. That is the energy necessary to bring the system from its initial equilibrium coordinates to the final ones without changing the total charge of each of the reactants. The inner-sphere reorganization energies were calculated as differences in total energies of ground states of $Fe^{II}Fe^{III}$ and $Fe^{III}Fe^{III}$ complexes at their equilibrium coordinates keeping for both of them the state $Fe^{II}Fe^{III}$ (designated as $Fe^{II}Fe^{III} \rightarrow (Fe^{III}Fe^{III})^{red}$), and vice versa. The data are given in Table 4. The reorganization energies for $Fe^{II}Fe^{III} \rightarrow (Fe^{III}Fe^{III})^{red}$ and $Fe^{III}Fe^{III} \rightarrow (Fe^{II}Fe^{III})^{ox}$ transitions are of the same order of magnitude. Hence, the potential curves for these two states are more or less symmetric. That allows the use of the averaged value of the reorganization energy in the activation energy calculations. It is remarkable that the reorganization energy for the fully optimized minimal complex is substantially higher than for the partly optimized one. This is the result of restrictions of the ligands' movements imposed by protein. Reorganization energies for the fully optimized minimal complex calculated by Sigfridsson et al. [22], viz. 18.3 kJ/mol and 21.8 kJ/mol, are fairly close to ours.

Table 4
Inner-sphere reorganization energies (kJ mol^{-1}) for MinC and ExtC complexes calculated at the B3LYP/6-31G(d,p) level.

	$Fe^{II}Fe^{III} \rightarrow (Fe^{III}Fe^{III})^{red}$	$Fe^{III}Fe^{III} \rightarrow (Fe^{II}Fe^{III})^{ox}$
MinC (partly optimized)	12.5	16.7
MinC (fully optimized)	16.6	20.9
ExtC (partly optimized)	12.3	17.7
ExtC, mono-deprotonated (partly optimized)	14.6	20.9
ExtC, bis-deprotonated (partly optimized)	15.4	24.4

The results with 6-31++G(d,p) basis differ less than by 2 kJ mol^{-1}.

3.2. Calculations of redox potentials

3.2.1. The scale of redox potentials

The standard electrode potential E_0 of a redox couple relative to the standard hydrogen electrode (S.H.E.) can be calculated according to the following formula:

$$FE_0 = \Delta G_{ion}(\mathrm{Red}) - [\Delta G_{solv}(\mathrm{Red}) - \Delta G_{solv}(\mathrm{Ox})] - FE(H) \quad (10)$$

where F is the Faraday constant, ΔG_{ion}(Red) is the standard Gibbs energy of ionization of the reduced form, ΔG_{solv}—the standard solvation Gibbs energies of the reduced and oxidized forms respectively, and the constant E(H) is determined by the following relationship:

$$FE(H) = {}^1/_2\Delta G_{diss}(H_2) + \Delta G_{ion}(H) + \Delta G_{hydr}(H^+) \quad (11)$$

involving standard Gibbs energies of the hydrogen molecule dissociation, the hydrogen atom ionization, and the proton hydration. For $E(H)$ the value 4.44 V is often employed. However, that is incorrect.

This potential that was first proposed by Kanevskii (E_K) [66–68] can be calculated in a thermodynamically rigorous way on the basis of experimental data as the sum of the metal work function and the metal/solution contact potential difference (Volta potential) at the potential of S.H.E. This quantity was called "the absolute electrode potential of the S.H.E". However, it was shown [69,70] that this definition is a conditional one because Kanevskii potential involves the "real" hydration energy which differs from the "chemical" energy $\Delta G_{hydr}(H^+)$ by the work of charge transfer across the water surface potential $\chi(H_2O)$:

$$\Delta G^{real}_{hydr}(H^+) = \Delta G_{hydr}(H^+) + F\chi(H_2O). \quad (12)$$

The surface potential depends on the water structure as well as on the presence of surface active substances even in so small concentrations that they do not influence the *emf* of a galvanic cell. Later, Reiss and Heller [71] have obtained practically the same value (4.43 V) using a more complicated reasoning. Newertheless, the physical meaning of their "absolute potential" is identical to that of Kanevskii [72].

As it was stressed in our previous paper [31], both half-reactions implied in Eq. (10) should be treated in a uniform way, i.e. for potentials of the electrode of interest and of the S.H.E. only "chemical" solvation energies should be employed. Therefore, in Eq. (11) enters the so-called Trasatti potential (E_T) [73,74] that differs from the Kanevskii potential by the surface potential of water: $E_K = E_T + \chi(H_2O)$ (the meaning of these two potentals is considered in detail in [75]).

The determination of the water/gas potential drop $\chi(H_2O)$ requires the use of some extrathermodynamic assumption. One of them based on the experimental real solvation energies and calculation of chemical energies for ferricenium ion was used in [76,77], where the following value was found: $\chi(H_2O) = +0.16$ V [77]. By virtue of the approximations made this estimate can be considered rather as the upper limit of this quantity. The probable lower limit, viz. $\chi(H_2O) = +0.13$ V gives the estimate done by Trasatti [78] on the basis of quite different assumptions. Consequently, Trasatti potential of the S.H.E. can be estimated as 4.30 ± 0.02 V. This value was employed in our subsequent calculations.

Solvation energies of reduced and oxidized forms in protein consist of two components: the dielectric response energy and the energy in the intraprotein electric field of the charges added to each atom upon redox reaction. All the energy contributions necessary to calculate redox potential are summarized in the subsequent tables.

3.2.2. Redox potential of the protonated form

As it was mentioned before, we have considered two models of the ISP redox center. First, the minimal complex (MinC) that included [2Fe2S] cluster with two imidazols and two methylsulfides mimicking His and Cys ligands of Fe atoms. In this model, the effect of Ser154 forming hydrogen bond to S is considered a purely electrostatic one (Table 5). The second model—extended complex (ExtC)—involves also Ser mimicked by methanol (Table 6). The second model is closer to the real situation, and hence seems to be more attractive.

As it was described in the Section 2.2, in the model of polarizable solute the effective charges should be increased in comparison to charges calculated quantum-chemically. Nevertheless, we present in Tables 5–7 the main results of calculations with corrected charges and also results obtained with uncorrected charges (vacuum charges). The latter differs from the more rigorous data by few tens of millivolts. This shows that the possible error introduced by approximation used upon evaluation of corrected charges is not large. The vacuum charges will be used in calculations of redox potentials of deprotonated forms (see below, Section 3.2.3).

The ionization energies obtained with 6-31G(d,p) set are substantially lower than those obtained with TZVP and 6-31++G(d,p) sets (Table 3). In all the cases, the redox potentials calculated with the energies of the 6-31G(d,p) set are in a much worser agreement with the experiment than those obtained with the two other basis sets. On this reason, only the latter are given in all subsequent tables.

Ionization potential for ExtC is by 0.24–0.26 eV higher than for MinC. This is understandable because hydrogen bond stabilizes the $Fe^{II}Fe^{III}$ state. However, this increase in ionization potential is overcompensated by lower electrostatic contributions. Indeed, in ExtC the total charge is distributed over a larger volume, and hence the dielectric response energy decreases. Besides that, in ExtC electrostatic interaction between Ser154 and other atoms of the complex are included in the full energy computed quantum-chemically while with MinC it is involved explicitly in the effect of the intraprotein electric field. As a result, the redox potentials calculated for MinC are more positive than that for ExtC (Tables 5, 6).

The static dielectric permittivity measured with dry proteins lies usually around 3.5–4. The last value is commonly employed in the corresponding electrostatic calculations. However, this value presents the quantity averaged over the whole protein globule. There are several molecular dynamic simulations showing that the dielectric permittivity of the outer part of a globular protein is higher than that of its core [79–85]. Though these results cannot be considered as strictly quantitative because these MD simulations have not taken into account explicitly the electronic polarizability of molecules, the existence of this effect seems to be reasonable. The first direct experimental evidence of an enhanced permittivity in the active site region of α-chymotrypsin has been obtained in [86] from the Stokes shift of the fluorescence spectrum of the dye proflavine sorbed in the binding pocket of α-chymotrypsin. Calculations of p*K* of the active site of α-chymotrypsin have shown that the best agreement with the experiment can be achieved when an effective uniform dielectric permittivity about 5 is ascribed to the protein globule [33].

The redox center of the Rieske ISP lies close to the globule surface. Therefore, we can expect that the effective dielectric permittivity is higher than 4. That was the reason to perform calculations also with $\varepsilon_{s,p}=5$. We are quite aware that this is not an exact figure. However, it should reflect the real trend and give the probable order of magnitude of the effect of an increase in dielectric permittivity.

The experimental value of redox potential of the fully protonated Rieske protein given in [8,87] is 0.308 V. This quantity was obtained using the protein film voltammetry (PFV). In principle, this method can bring about some error due to the protein–adsorbent interactions. However, as it was shown in [88] on example of another ISP, the experimental technique employed in these works (PFV without usage of adsorption promotors) gives results coinciding in limits of few millivolts with those obtained by classical cyclic voltammetry, i.e. related to the dissolved protein. Further, the CD-monitored redox titration of Rieske ISP in situ in bc_1 complex gives potentials of 0.315 V [87,89] or 0.312 V [90] (some difference from the potential of the isolated protein seems to be reasonable). In all the papers quoted, the standard deviation was estimated as ±5 mV. On the basis of these considerations, we can accept for the redox potential of the fully protonated Rieske ISP the value of 0.31 V. There is no reason to employ as the reference point the experimental potentials with the accuracy

Table 6
Calculations of redox potential for the extended complex.

			$\varepsilon_{s,p}=4$	$\varepsilon_{s,p}=5$
Difference of dielectric response energies, eV $Fe^{III}Fe^{III}$–$Fe^{II}Fe^{III}$	Calculations with vacuum charges		1.453	1.526
	Calculations with modified charges		1.508	1.580
Effect of the intraprotein field, eV			0.940	
Gibbs free energy of ionization, eV		I	2.043	
		II	2.115	
Redox potential, V	Calculations with vacuum charges	I	0.136	0.209
		II	0.208	0.281
	Calculations with modified charges	I	0.191	0.263
		II	0.263	0.335

I—ionization energy calculated with the TZVP basis set, II—the same with the 6-31++G(d,p) basis set.

Table 5
Calculations of redox potential for the partly optimized minimal complex.

			$\varepsilon_{s,p}=4$	$\varepsilon_{s,p}=5$
Difference of dielectric response energies, eV $Fe^{III}Fe^{III}$–$Fe^{II}Fe^{III}$	Calculations with vacuum charges		1.795	1.790
	Calculations with modified charges		1.780	1.826
Effect of the intraprotein field, eV			1.025	
Gibbs free energy of ionization, eV		I	1.784	
		II	1.871	
Redox potential, V	Calculations with vacuum charges	I	0.304	0.299
		II	0.391	0.386
	Calculations with modified charges	I	0.289	0.335
		II	0.376	0.422

I—ionization energy calculated with the TZVP basis set, II—the same with the 6-31++G(d,p) basis set.

Table 7
Calculations of redox potential for the fully optimized minimal complex.

			$\varepsilon_{s,p}=4$	$\varepsilon_{s,p}=5$
Difference of dielectric response energies, eV $Fe^{III}Fe^{III}$–$Fe^{II}Fe^{III}$	Calculations with vacuum charges		1.521	1.598
	Calculations with modified charges		1.561	1.662
Effect of the intraprotein field, eV			0.897	
Gibbs free energy of ionization, eV		I	1.813	
		II	1.893	
Redox potential, V	Calculations with vacuum charges	I	−0.069	0.008
		II	0.011	0.088
	Calculations with modified charges	I	−0.029	0.072
		II	0.051	0.152

I—ionization energy calculated with the TZVP basis set, II—the same with the 6-31++G(d,p) basis set.

better than 0.01 V. The similarly rounded figures are used throughout in this paper.

The calculated potentials (Tables 5, 6) are of correct order of magnitude but for different parameters they deviate more or less from 0.31 V both in negative and positive directions.

It is difficult to prefer a priori the employment of TZVP or 6-31++G (d,p) basis sets (versions I and II in Tables 5–7). The experimental redox potential 0.31 V is rather close to quantities calculated in version II for ExtC with modified charges (0.263 V and 0.335 V at $\varepsilon_s = 4$ and 5, correspondingly), for MinC the best results were obtained with the TZVP set (variations from 0.289 V to 0.335 V). In total, these figures are rather close to the experimental value; keeping in mind all approximations inherent to these calculations we can conclude that the agreement is in fact even better than could be expected.

Some tendencies can be traced. Employment of the corrected charges shifts the calculated potential towards positive values; as a rule, the positive shift is also observed with the effective dielectric permittivity increasing. The scatter of the data does not allow us to chose confidently between two models—ExtC and MinC, but the first one is nearer to the real structure of the active site.

As it was mentioned before, the active site structure inside the protein differs markedly from the structure of the same complex optimized in vacuum. This results in a substantial difference in their energies (cf. Tables 5 and 7). The ionization free energy of the fully optimized complex is slightly higher than for the complex constrained by protein. However, the partial charge distribution in the fully optimized complex is more uniform than in the complex which structure is affected by protein. As a result, the components of electrostatic energies for the optimized complex are substantially smaller; consequently, the calculated redox potentials are ~0.26 V ($\varepsilon_{s,p} = 4$) or ~0.32 V ($\varepsilon_{s,p} = 5$) more negative as compared to those calculated for the partly optimized complex (the difference is practically the same for both basis sets). The potentials calculated for the partly optimized complex are much closer to the experimental data than those for the fully optimized complex. Therefore, we can conclude that the effect of the protein matrix on the active site structure plays an important role in tuning the redox potential.

A detailed quantum-chemical/electrostatic analysis for the bovine Rieske ISP was done previously by Ullmann et al. [15]. They used somewhat different models and different quantum-chemical approaches. Redox potential for the fully protonated form calculated in this work was by 0.32 V more negative than the experimental value while in the present paper we have found, with the optimal set of parameters, the difference of −0.04 V/+0.03 V. Unfortunately, in [15], the main energy components involved in calculations such as ionization potential and electrostatic energies are not given explicitly. Hence it is difficult to make a detailed comparison of our results with those of [15]. One of the important reasons for their discrepancy lies in the value of the absolute electrode potential of SHE accepted: the figure employed in this work is, as discussed above, by 0.13 V lower than that used in [15]. Another possible source of the difference is the employment of the optical dielectric permittivity in our calculations of the intraglobular electric field while in [15], most probably, the static value was used. As it is shown below, this correction to the field effect plays a substantial role (see Section 3.2.5).

3.2.3. Redox potentials of the deprotonated extended complexes

Deprotonated complexes in reduced and oxidized forms bear charges of −2 and −1 (mono-deprotonated) or −3 and −2 (bis-deprotnated) correspondingly. Thus, there is no neutral molecule, and hence it is impossible to estimate modified charges in the way employed for the oxidized protonated complex. Therefore, we had to restrict ourselves with more approximate calculations using unmodified charges only. However, as it is seen from Tables 5–7, results with modified and unmodified (vacuum) charges differ not so strongly. This makes the approximation employed acceptable.

Fully deprotonated reduced and oxidized forms of Rieske protein exist at strongly alkaline pH. The p*K*'s of these forms are estimated in [87] as 12.4. The redox potentials were determined experimentally up to pH 14. Under these conditions, side chains of lysines are neutral. The p*K* of free arginine equal to 12. Keeping in mind the possibility of some shift of the Arg's p*K* in protein, we cannot be sure that arginines are fully deprotonated in vicinity of pH 12.4. Therefore, the calculation of the intraprotein electric field in alkaline solutions was performed in two versions—with both lysines and arginines neutral, and with only lysines deprotonated. The effect of the positive charges of all arginines is found to be 0.07 V. With partly dissociated arginines, their contribution making up only a fraction of this quantity.

The results of our calculations are given in Table 8 for both steps of acid dissociation. For the first step, deprotonation at His 152 is considered as the only physiologically relevant. Due to high charges of all species, the dielectric response energies are large, and the final result is more sensitive to the choice of dielectric permittivity. The direct experimental data available relate to a fully deprotonated form. The corresponding value of the redox potential is −0.13 V [87]. The closest to this figure result of calculations was obtained with TZVP basis set at $\varepsilon_{s,p} = 5$ (−0.156 V; in these calculations, all arginines were accepted to be neutral; if they are partly charged, the potential will shift to positive by few tens of millivolts). The scatter of calculated values is rather large.

Keeping in mind the employment of vacuum charges, it is interesting to compare not only the absolute values of potentials but also their difference for protonated and bis-deprotonated forms calculated in the framework of the same approximations, viz. with vacuum charges and with the TZVP basis set. Corresponding difference equals to −0.487 V at $\varepsilon_{s,p} = 4$ and −0.365 V at $\varepsilon_{s,p} = 5$. The agreement of these figures with the experimental difference −0.44 V [87] seems to be reasonable. With the 6-31++G(d,p) basis set the difference is smaller, −0.299 V and −0.261 V correspondingly.

One problem should be mentioned here. In our electrostatic calculations, we used the experimental coordinates of all atoms, both in active site and in matrix. The X-ray structures were determined with the protonated form of the Rieske protein. The calculations of structures of the isolated complex have revealed some marked differences between protonated and deprotonated forms (Table 1, Section 3.1.1). On the other hand, the protein structure should change somewhat upon charging and deprotonation of the active site. All these effects cause, in principle, some errors in electrostatic calculations, the errors that cannot be estimated a priori.

3.2.4. Redox potential of mutants

The mutant Y156F has a structure practically identical with that of the wild type [8]. Tyr156 forms hydrogen bond with S of Cys149, i.e. not with the core of cluster. Hence, one could suppose that its effect on

Table 8
Calculations of redox potential for the deprotonated extended complexes (only vacuum charges used).

		Mono-deprotonated complex		Bis-deprotonated complex	
		$\varepsilon_{s,p} = 4$	$\varepsilon_{s,p} = 5$	$\varepsilon_{s,p} = 4$	$\varepsilon_{s,p} = 5$
Difference of dielectric response energies, eV $Fe^{III}Fe^{III}$–$Fe^{II}Fe^{III}$		4.176	4.266	6.885	6.996
Effect of the intraprotein field, eV		0.799		0.784	
Gibbs free energy of ionization, eV	I	−0.903		−3.636	
	II	−0.791		−3.460	
Redox potential, V	I	−0.228	−0.138	−0.361	−0.156
	II	−0.116	−0.026	−0.091	0.020

I—ionization energy calculated with the TZVP basis set, II—the same with the 6-31++G(d,p).

the redox potential of the active site is predominantly the electrostatic one, and we do not need an additional quantum-chemical analysis of the system. So, we can accept that the ionization potential of the ExtC remains the same as well as the partial charge distribution in the complex. The last means that the dielectric response energy is unchanged, and the only factor influencing the result is the change of the intraprotein electric field due to substitution of Phe for Tyr. Accepting the protein matrix structure unchanged, the calculated effect results in a shift of potential by −49 mV, in a good agreement with the experimental shift equal to −56 mV [90].

A different situation takes place with the S154A mutant. In this case, the protein structure was found to be the same, in limits of experimental errors, as for the wild type [8]. However, substitution of Ala for Ser eliminates the hydrogen bond with the [2Fe2S] cluster. Therefore, the proper model of the redox center for this mutant is the MinC. In comparison to the field effect of Ser154, the effect of Ala is by 84 meV lower (a negative contribution to redox potential). The calculated redox potential for this mutant (using modified charges and $\varepsilon_{s,p}=5$) with the ionization energies calculated at the TZVP atomic basis set is 0.251 V, and at the 6-31++G(d,p) basis set is 0.338 V. This is by 12 mV more negative and by 3 mV more positive than the values calculated with the same parameters for the wild type. This differs markedly from the experimentally observed negative shift by 135 meV [8]. The probable reasons for this discrepancy seem to be as follows. The calculated difference involves the errors in two quantum-chemically calculated energies of complexes of different compositions and structures, viz. MinC and ExtC. Probably, these errors have not compensated each other. Note that the small mutant's effects are the difference of large items, and hence are sensitive even to small relative errors in calculations. The second possible cause of error is some inaccuracy in protein coordinates. It seems probable that, due to loss of the hydrogen bond with the [2Fe2S] core, position of aminoacid residues closest to the active site may change affecting the value of the intraprotein electric field.

In the mutant Y156W the backbone configuration is somewhat changed as compared to the wild type. This is due to a substantially larger size of the tryptophan residue that cannot fit into the space occupied by tyrosine. As a result, the whole redox center is shifted by 0.4 Å [8]. Upon this shift, the distances in the [2Fe2S] cluster between Fe and all ligands, and Oγ Ser154–S2 remain constant in the limits of 0.01 Å. However, the ligands' mutual orientation changes, e.g., the distance between two Cβ atoms of Cys129 and Cys149 increases from 4.26 Å to 4.41 Å. Therefore, a new quantum-chemical analysis was performed. Ionization potential decreased by −0.18 eV (TZVP) or by 0.16 eV (with 6-31++G(d,p) basis) that gives the equivalent negative shift of redox potential. The change of the intraprotein electric field effect was found to be equal to −0.143 eV; that is due to disappearance of the OH dipole and to somewhat increased distance between the active site and some backbone dipoles. However, the partial charge distribution in the mutated complex differs markedly from that in ExtC. As a result, the dielectric response energy that is sensitive to charge distribution increases by 0.22–0.26 eV ($\varepsilon_{s,p}=4$ and $\varepsilon_{s,p}=5$ correspondingly, modified charges). The calculated redox potential at $\varepsilon_{s,p}=5$ with TZVP is 0.200 V, and with 6-31++G(d,p) 0.292 V, the calculated shift relative to WT is −0.063 V and −0.043 V correspondingly; at $\varepsilon_{s,p}=4$ the calculated shifts are −0.103 V and −0.086 V. The experimental redox potential equals 0.20 V [87], i.e. a negative shift by 0.11 V is observed. The calculated figures demonstrate a reasonable agreement with the experiment, correct in sign and in order of magnitude. This differs from the case of the S154A mutant discussed above. In contrast to the latter, in the Y156W mutant we deal with the active complex of the same chemical composition both in the wild type and mutated protein. This should decrease the relative errors in calculations of their ionization potentials. Further, the change in the protein structure upon mutation was accounted for explicitly.

3.2.5. Optical dielectric permittivity in calculation of the intraprotein electric field

As it was stated in the Section 2, the intraprotein electric field was calculated using the optical dielectric permittivity of protein and the static one of water. The physical reason for that is as follows. The partial charges of the protein atoms exert the effects of two kinds: they create an intraprotein electric field, and the shift of their equilibrium positions in response to an electric field constitutes the inertial part of the protein's dielectric response. The full dielectric response described by the protein's static dielectric permittivity involves both electronic and atomic polarizations. When in calculation of the intraprotein electric field the static dielectric permittivity is employed (this is a traditional approach) one accounts twice for the effect of partial charges: as a source of the field, and as a self-screening polarization [83]. This contradiction was resolved in [32]. At a given protein structure, the coordinates of all atoms are fixed, and hence the dielectric screening of the pre-existing field does not involve dielectric response due to the shift of atoms. Hence, only electronic polarization affects the pre-existing field. Therefore, within the framework of the semi-continuum formalism, the intraprotein electric field should be calculated using the protein's optical dielectric permittivity $\varepsilon_{o,p}$. Positions of water molecules surrounding the protein globule are not fixed, and therefore the screening of the intraprotein field by this external medium should be calculated using the water's static dielectric permittivity $\varepsilon_{s,w}$.

The dielectric response energy includes the interaction of the newly formed charge with all kinds of polarization induced by this charge, hence also that due to the shift of all protein's atoms. This component should be calculated using the static dielectric permittivity $\varepsilon_{s,p}$ (and, of course, $\varepsilon_{s,w}$).

The approach described above was successfully applied to calculations of p*K* of the active site of α-chymotrypsin [33] and of redox potentails of all cofactors in Photosystem I [24].

The use of two dielectric permittivities was proposed also by Simonson et al. [91]. In this work, the static dielectric permittivity was used for calculation of charging energy while for the pre-existing field the choice was not so definite. The authors preferred to use the value of $\varepsilon_{i,p}$ close to 1, neglecting thereby practically the medium electronic polarization.

For the sake of comparison, we have performed some calculations of the intraglobular electric field for our object using the static dielectric permittivity of protein $\varepsilon_{s,p}=4$. For ExtC, the effect of electric field was revealed to be 0.345 eV lower than at $\varepsilon_{o,p}=2.5$. The redox potential calculated with this field varies, depending on the parameter set chosen, between −0.01 V and −0.209 V, i.e. the discrepancy with the experiment is very large. The employment of $\varepsilon_{i,p}=1$ produces an effect of the opposite sign—an increase in redox potential by 0.46 V that is in a drastic contradiction with the experimental value. Much worser estimates of mutation effects were also observed using for $\varepsilon_{i,p}$ values of 4 or 1. So, similar to results obtained in the papers quoted above the best agreement with the experiment was achieved while in calculation of the intraprotein electric field the optical dielectric permittivity was employed.

4. Conclusions

The combined quantum-chemical and electrostatic calculation of the redox potentials of the Rieske ISP results in a reasonable agreement with the experiment, as a rule substantially better than was achieved earlier in calculations of the kind for various iron–sulfur proteins (e.g., in [14–16] most calculated figures deviate from the experimental ones by ~0.3 V and even more). This is seen from Table 9 where experimental data are compared with the theoretical ones obtained using the optimal sets of parameters. The worst agreement was observed for the S154A mutant. In this case, the mutated protein structure was described as being the same as for the wild type what is definitely not true. A similar problem, namely the

Table 9
Comparison of the experimental and calculated redox potentials; in V.

The Rieske ISP	Experimental redox potentials	Redox potentials calculated at $\varepsilon_{s,p}=5$ with the two atomic basis sets	
		TZVP	6-31++G(d,p)
Wild type, protonated	0.31 [8,87,89,90]	0.263	0.335
Wild type, bis-deprotonated	−0.13 [87]	−0.156	0.020
S154A, protonated	0.17 [8]	0.251	0.338
Y156F, protonated	0.26 [90]	0.214	0.286
Y156W, protonated	0.20 [90]	0.200	0.292

change of the protein structure in strongly alkaline solutions, decreases the accuracy of calculations for the bis-deprotonated WT.

In our continuum electrostatic calculations of the dielectric response energy we employed the model of the polarizable solute (with the correspondingly modified partial charges). This model accounts for the solute electronic polarization in an external electric field. The effect of the intraprotein electric field was computed using the protein's optical dielectric permittivity, while the dielectric reponse energies were calculated employing the static permittivity. In this way, the two different phenomena—the shift of the atomic partial charges contributing to the response energy, and the effect of these charges as the sources of the intraprotein electric field are accounted for separately. Both these specific features have a clear physical substantiation, and only their employment provides a reasonble agreement with the experiment.

The static dielectric permittivity of protein is inhomogeneous, the outer part of the globule has a higher permittivity due to an enhanced mobility of residues near the protein surface. This effect was approximated by employing an effective $\varepsilon_{s,p}=5$ instead of the traditional value $\varepsilon_{s,p}=4$, the latter being an average over the whole protein's body. This enhanced value of permittivity results in general in better agrement with the experiment.

An important feature of our calculation is the choice of the value of the absolute electrode potential of S.H.E. In contrast to commonly accepted figures of 4.43–4.44 V, we used the so-called "Trasatti potential" 4.30 V which includes the correction for the surface potential at the water/gas boundary, the correction that is necessary from the physical point of view.

Redox potential of the Rieske ISP is substantially more positive than for other proteins containing [2Fe2S] clusters. This is due first of all to its high ionization potential. In contrast to $Fe_2S_2Cys_4$ clusters, the active site of Rieske ISP contains two uncharged His ligands. Therefore, the total charge decreases; for protonated form ionization of the $Fe^{II}Fe^{III}$ state corresponds to a −1/0 transition, and for deprotonated forms to −2/−1 and −3/−2 transitions. The corresponding gas phase ionization free energies are +2.04 eV, −0.90 eV and −3.64 eV for the the TZVP basis set; the values for 6-31++G(d,p) set are +2.12 eV, −0.79 eV, and −3.46 eV. Not only does the total charge play the role but the nature of ligands too. So, for $Fe_2S_2Cys_4$ cluster the −3/−2 transition has the ionization potential of about −5 eV [13]. One should note also that the hydrogen bond of Ser154 to one of the S atoms of the [2Fe2S] cluster increases markedly the ionization potential (by 0.24–0.26 eV for the protonated form).

The great differences in ionization potentials of different ionic forms are largely compensated for by an increase in the dielectric response energy with an increasing charge of the complex; however, this compensation is not a complete one. The response energy is determined not by an additional charge (which is in all cases the same, viz. 1) but by the total charge of the particle. Indeed, the charging energy is quadratic relative to charge, and hence the energy difference between $Fe^{II}Fe^{III}$ and $Fe^{III}Fe^{III}$ states increases with the total charge increasing. It is interesting that even for a neutral $Fe^{III}Fe^{III}$ state its charging energy is substantial due to many partial charges distributed rather asymmetrically. So, the difference in the dielectric response energies of protonated $Fe^{II}Fe^{III}$ and $Fe^{III}Fe^{III}$ complexes equals to 1.51 eV (at $\varepsilon_{s,p}=4$, modified charges) while the dielectric response due to the excessive partial charges only (their sum is −1) is 1.39 eV. We have shown earlier [31] that for very symmetric metallocene systems the difference in the dielectric response energies for +1 and 0 states practically coincides with the dielectric response energy for an excessive charge only. However, for an asymmetric structure this is not the case.

The values of the ionization potentials computed quantum-chemically are one of the main sources of errors in the absolute calculation of redox potentials. Therefore, it is desirable to exclude, if possible, these quantities from the final analysis. This could be in principle done when the direct experimental data on the redox potential of a model compound in some, preferably aprotic, solvent are available. In this case, one does not need to perform the absolute calculation of the redox potential as it was done in the present work, but only its shift in protein relative to that in solvent should be calculated; essentially, the electrostatic transfer energies are to be computed. With the Rieske ISP the corresponding data are absent but such kind of calculations was performed successfully for [4Fe4S] clusters in Photosystem I and some ferredoxins [20].

It is important to note that the quantitative electrostatic calculation of the transfer energy implies that the structure of the active site and charge density distribution inside it are the same (or at least rather similar) in protein and in solvent. These parameters for dissolved model compound are, most probably, similar to those for the molecule optimized in the gas phase. As it was shown in the present study, the structure of the redox center in the Rieske ISP deviates markedly from the structure of its model optimized in the gas phase due to constraints imposed by the protein structure. This affects its ionization potential and, via the influence on the partial charge distribution, electrostatic components of energy. Our calculations performed with the fully optimized structure of the active site has shown that both the ionization potential and, especially, the change of electrostatic contributions shift the calculated redox potential by 0.26–0.32 V (modified charges). This demonstrates that the distortion of the active site structure plays a substantial role in tuning of the redox potential.

The same effect of the structure distortion may influence also the redox potentials of mutants. Not only the change in the chemical composition of the active site but also some change in its configuration due to the stress imposed by the change of the protein conformation results in marked effects. Therefore, while doing electrostatic calculations, one should keep in mind the possibility of interference of various structural effects, and in each particular case this problem should be explored especially.

Acknowledgements

The work was supported by the Russian Foundation for Basic Research (Grant No. 09-03-00085-a).

Appendix A. Supplementary data

Supplementary data associated with this article can be found, in the online version, at doi:10.1016/j.bbabio.2009.12.004.

References

[1] A.R. Crofts, E.A. Berry, Structure and function of the cytochrome *bc*(1) complex of mitochondria and photosynthetic bacteria, Curr. Opin. Struct. Biol. 8 (1998) 501–509.
[2] E.A. Berry, M. Guergova-Kuras, L.S. Huang, A.R. Crofts, Structure and function of cytochrome *bc* complexes, Ann. Rev. Biochem. 69 (2000) 1005–1075.
[3] C. Hunte, Insights from the structure of the yeast cytochrome *bc*1 complex: crystallization of membrane proteins with antibody fragments, FEBS Lett. 504 (2001) 126–132.

[4] E. Darrouzet, C.C. Moser, P.L. Dutton, F. Daldal, Large scale domain movement in cytochrome *bc*1: a new device for electron transfer in proteins, TRENDS Biochem. Sci. 26 (2001) 445–451.
[5] A.R. Crofts, Proton-coupled electron transfer at the Qo-site of the *bc*1 complex controls the rate of ubihydroquinone oxidation, Biochim. Biophys. Acta 1655 (2004) 77–92.
[6] S. Iwata, M. Saynovits, T.A. Link, H. Michel, Structure of a water soluble fragment of the 'Rieske' iron–sulfur protein of the bovine heart mitochondrial cytochrome *bc*1 complex determined by MAD phasing at 1.5 Å resolution, Structure 4 (1996) 567–579.
[7] C.J. Carrell, H. Zhang, W.A. Cramer, J.L. Smith, Biological identity and diversity in photosynthesis and respiration: structure of the lumen-side domain of the chloroplast Rieske protein, Structure 5 (1997) 1613–1625.
[8] D.J. Kolling, J.S. Brunzelle, S.M. Lhee, A.R. Crofts, S.K. Nair, Atomic resolution structures of Rieske iron–sulfur protein: role of hydrogen bonds in tuning the redox potential of iron–sulfur clusters, Structure 15 (2007) 29–38.
[9] E.T. Smith, J.M. Tomich, T. Iwamoto, J.H. Richards, Y. Mao, B.A. Feinberg, A totally synthetic histidine-2 ferredoxin: thermal stability and redox properties, Biochemistry 30 (1991) 11669–11676.
[10] R. Langen, G.M. Jensen, U. Jacob, P.J. Stephens, A. Warshel, Protein control of iron–sulfur cluster redox potentials, J. Biol. Chem. 267 (1992) 25625–25627.
[11] G.M. Jensen, A. Warshel, P.J. Stephens, Calculation of the redox potentials of iron–sulfur proteins: the 2−/3− couple of [Fe4S4Cys4] clusters in *Peptococcus aerogenes* ferredoxin, Azotobacter vinelandii ferredoxin I, and Chromatium vinosum high-potential iron protein, Biochemistry 33 (1994) 10911–10924.
[12] P.J. Stephens, D.R. Jollie, A. Warshel, Protein control of redox potentials of iron–sulfur proteins, Chem. Rev. 96 (1996) 2491–2513.
[13] J.-M. Mouesca, J.L. Chen, L. Noodleman, D. Bashford, D.A. Case, Density functional/Poisson–Boltzmann calculations of redox potentials for iron–sulfur clusters, J. Am. Chem. Soc. 116 (1994) 11898–11914.
[14] J. Li, M.R. Nelson, C.Y. Peng, D. Bashford, L. Noodleman, Density functional/Poisson–Boltzmann calculations of redox potentials for iron–sulfur clusters, J. Phys. Chem. A 102 (1998) 6311–6324.
[15] G.M. Ullmann, L. Noodleman, D.A. Case, Density functional calculation of pK_a values and redox potentials in the bovine Rieske iron–sulfur protein, J. Biol. Inorg. Chem. 7 (2002) 632–639.
[16] R.A. Torres, T. Lovell, L. Noodleman, D.A. Case, Density functional and reduction potential calculations of Fe_4S_4 clusters, J. Am. Chem. Soc. 125 (2003) 1923–1936.
[17] C.C. Correll, M.L. Ludwig, C.M. Bruns, P.A. Karplus, Structural prototypes for an extended family of flavoprotein reductases: comparison of phthalate dioxygenase reductase with ferredoxin, reductase and ferredoxin, Protein Sci. 2 (1993) 2112–2133.
[18] L. Banci, I. Bertini, G. Gori Savellini, C. Luchinat, Individual reduction potentials of the iron ions in Fe2S2 and high-potential Fe4S4 ferredoxins, Inorg. Chem. 35 (1996) 4248–4253.
[19] B.W. Beck, Q. Xie, T. Ichiye, Sequence determination of reduction potentials by cysteinyl hydrogen bonds and peptide dipoles in [4Fe–4S] ferredoxins, Biophys. J. 81 (2001) 601–613.
[20] V.V. Ptushenko, D.A. Cherepanov, L.I. Krishtalik, A.Yu. Semenov, Semi-continuum electrostatic calculations of redox potentials in photosystem I, Photosynth. Res. (2008) 55–74.
[21] A.R. Klingen, G.M. Ullmann, Negatively charged residues and hydrogen bonds tune the ligand histidine pK_a values of Rieske iron–sulfur proteins, Biochemistry 43 (2004) 12383–12389.
[22] E. Sigfridsson, M.H.M. Olsson, U. Ryde, Inner-sphere reorganization energy of iron–sulfur clusters studied with theoretical methods, Inorg. Chem. 40 (2001) 2509–2519.
[23] A. Bassan, M.R.A. Blomberg, T. Borowski, P.E.M. Siegbahn, Oxygen activation by Rieske non-heme iron oxygenases, a theoretical insight, J. Phys. Chem. B 108 (2004) 13031–13041.
[24] M. Shoji, K. Koizumi, Y. Kitagawa, S. Yamanaka, M. Okumura, K. Yamaguchi, Theory of chemical bonds in metalloenzymes IV: Hybryd-DFT study of Rieske-type [2Fe–2S] clusters, Int. J. Quant. Chem. 107 (2007) 609–627.
[25] L. Noodleman, J.G. Norman Jr., The X_α valence bond theory of weak electronic coupling. Application to the low-lying states of $Mo_2Cl_8^{4-}$, J. Chem. Phys. 70 (1979) 4903–4906.
[26] L. Noodleman, Valence bond description of antiferromagnetic coupling in transition metal dimers, J. Chem. Phys. 74 (1981) 5737–5743.
[27] L. Noodleman, E.J. Baerends, Electronic structure, magnetic properties, ESR, and optical spectra for 2-Fe ferrodoxin models by LCAO-X_α valence bond theory, J. Am. Chem. Soc. 106 (1984) 2316–2327.
[28] L. Noodleman, E.R. Davidson, Ligand spin polarization and antiferromagnetic coupling in transition metal dimers, Chem. Phys. 109 (1986) 131–143.
[29] L. Noodleman, D.A. Case, Density functional theory of spin polarization and spin coupling in iron–sulfur clusters, Adv. Inorg. Chem. 38 (1992) 423–470.
[30] L. Noodleman, C.Y. Peng, D.A. Case, J.-M. Mouesca, Orbital interactions, electron delocalization, and spin interactions in iron–sulfur clusters, Coord. Chem. Rev. 144 (1995) 199–244.
[31] An.M. Kuznetsov, A.N. Maslii, L.I. Krishtalik, Quantum chemical model of solvation for calculation of electrode potentials of redox processes involving ferrocene, cobaltocene, and their ions, Russ. J. Electrochem. 44 (2008) 34–42.
[32] L.I. Krishtalik, A.M. Kuznetsov, E.L. Mertz, Electrostatics of proteins: description in terms of two dielectric permittivitys simultaneously, Proteins: Struct. Funct. Genet. 28 (1997) 174–182.
[33] L.I. Krishtalik, Continuum electrostatics of proteins: experimental test with model solvents and the method of the proteins pK calculations, Chem. Phys. 319 (2005) 316–329.
[34] Gaussian 03, Revision C.01, M.J. Frisch, G.W. Trucks, H.B. Schlegel, G.E. Scuseria, M.A. Robb, J.R. Cheeseman, J.A. Montgomery, Jr., T. Vreven, K.N. Kudin, J.C. Burant, J.M. Millam, S.S. Iyengar, J. Tomasi, V. Barone, B. Mennucci, M. Cossi, G. Scalmani, N. Rega, G.A. Petersson, H. Nakatsuji, M. Hada, M. Ehara, K. Toyota, R. Fukuda, J. Hasegawa, M. Ishida, T. Nakajima, Y. Honda, O. Kitao, H. Nakai, M. Klene, X. Li, J.E. Knox, H.P. Hratchian, J.B. Cross, C. Adamo, J. Jaramillo, R. Gomperts, R.E. Stratmann, O. Yazyev, A.J. Austin, R. Cammi, C. Pomelli, J.W. Ochterski, P.Y. Ayala, K. Morokuma, G.A. Voth, P. Salvador, J.J. Dannenberg, V.G. Zakrzewski, S. Dapprich, A.D. Daniels, M.C. Strain, O. Farkas, D.K. Malick, A.D. Rabuck, K. Raghavachari, J.B. Foresman, J.V. Ortiz, Q. Cui, A.G. Baboul, S. Clifford, J. Cioslowski, B.B. Stefanov, G. Liu, A. Liashenko, P. Piskorz, I. Komaromi, R.L. Martin, D.J. Fox, T. Keith, M.A. Al-Laham, C.Y. Peng, A. Nanayakkara, M. Challacombe, P.M.W. Gill, B. Johnson, W. Chen, M.W. Wong, C. Gonzalez, and J.A. Pople, Gaussian, Inc., Wallingford CT, 2004.
[35] A. Becke, Density–functional thermochemistry. III. The role of exact exchange, J. Chem. Phys. 98 (1993) 5648–5652.
[36] C. Lee, W. Yang, R.G. Parr, Development of the Colle–Salvetti correlation-energy formula into a functional of the electron density, Phys. Rev. B. 37 (1988) 785–789.
[37] A. Schaefer, H. Horn, R. Ahlrichs, Fully optimized contracted Gaussian basis sets for atoms Li to Kr, J. Chem. Phys. 97 (1992) 2571–2577.
[38] A. Schaefer, C. Huber, R. Ahlrichs, Fully optimized contracted Gaussian basis sets of triple zeta valence quality for atoms Li to Kr, J. Chem. Phys. 100 (1994) 5829–5835.
[39] E. Ruiz, J. Cano, S. Alvarez, P. Alemany, Broken symmetry approach to calculation of exchange coupling constants for homobinuclear and heterobinuclear transition metal complexes, J. Comput. Chem. 20 (1999) 1391–1400.
[40] E. Ruiz, A. Rodrigues-Fortea, J. Cano, S. Alvarez, P. Alemany, About the calculation of exchange coupling constants in polynuclear transition metal complexes, J. Comput. Chem. 24 (2003) 982–989.
[41] P. Ghosh, E. Bill, T. Weyhermuller, F. Neese, K. Wieghardt, The non-innocence of the ligand Glyoxal-bis (2-mercaptoanil). The electronic structures of $[Fe(gma)]_2$, $[Fe(gma)(py)]^*py$, $[Fe(gma)(CN)]^{1-/0}$, $[Fe(gma)I]$, $[Fe(gma)(PR_3)_n]$ $(n=1,2)$. Experimental and theoretical evidence for 'excited state' coordination, J. Amer. Chem. Soc. 125 (2003) 1293–1308.
[42] U.C. Singh, P.A. Kollman, An approach to computing electrostatic charges of molecules, J. Comput. Chem. 5 (1984) 129–145.
[43] B.H. Besler, K.M. Merz Jr., P.A. Kollman, Atomic charges derived from semiempirical methods, J. Comput. Chem. 11 (1990) 431–439.
[44] D. Christen, J.H. Griffits, J. Sheridan, The microwave spectrum of imidazole; complete structure and the electron distribution from nuclear quadrupole coupling tensor and dipole moment orientation, Z. Naturforsch. A 36 (1981) 1378–1385.
[45] G.O. Sørensen, L. Mahler, N. Rastrup-Andersen, Microwave spectra of $[^{15}N]$ and $[^{13}C]$ pyridines, quadrupole coupling constants, dipole moment and molecular structure of pyridine, J. Mol. Struct. 20 (1974) 119–126.
[46] A. Nicholls, B. Honig, A rapid finite difference algorithm, utilizing successive over-relaxation to solve the Poisson–Boltzmann equation, J. Comput. Chem. 12 (1991) 435–445.
[47] S.J. Weiner, P.A. Kollman, D.A. Case, U.C. Singh, C. Ghio, G. Alagona, S. Profeta Jr., P. Weiner, A new force field for molecular mechanical simulation of nucleic acids and proteins, J. Am. Chem. Soc. 106 (1984) 765–784.
[48] W.D. Cornell, P. Cieplak, C.I. Bayly, I.R. Gould, K.M. Merz Jr., D.M. Ferguson, D.C. Spellmeyer, T. Fox, J.W. Caldwell, P.A. Kollman, A second generation force field for the simulation of proteins, nucleic acids, and organic molecules, J. Am. Chem. Soc. 117 (1995) 5179–5197.
[49] I.V. Leontyev, M.V. Vener, I.V. Rostov, M.V. Basilevsky, M.D. Newton, Continuum level treatment of electronic polarization in the framework of molecular simulations of solvation effects, J. Chem. Phys. 119 (2003) 8024–8037.
[50] M.V. Vener, I.V. Leontyev, M.V. Basilevsky, Computations of solvation free energies for polyatomic ions in water in terms of a combined molecular–continuum approach, J. Chem. Phys. 119 (2003) 8038–8046.
[51] I.V. Leontyev, M.V. Basilevsky, M.D. Newton, Theory and computation of electron transfer reorganization energies with continuum and molecular solvent models, Theor. Chem. Acc. 111 (2004) 110–121.
[52] D. Sitkoff, K.A. Sharp, B. Honig, Accurate calculation of hydration free energies using macroscopic solvent models, J. Phys. Chem. 98 (1994) 1978–1988.
[53] J. Tomasi, M. Persico, Molecular interactions in solution: an overview of methods based on continuous distributions of the solvent, Chem. Rev. 94 (1994) 2027–2094.
[54] C.J. Cramer, D.G. Truhlar, Implicit solvation models: equilibria, structure, spectra, and dynamics, Chem. Rev. 99 (1999) 2161–2200.
[55] Yu.I. Kharkats, L.I. Krishtalik, Medium reorganization energy and enzymatic reaction activation energy, J. Theor. Biol. 112 (1985) 221–249.
[56] L.I. Krishtalik, G.-S. Tae, D.A. Cherepanov, W.A. Cramer, The redox properties of cytochromes *b* imposed by the membrane electrostatic environment, Biophys. J. 65 (1993) 184–195.
[57] G.M. Soriano, W.A. Cramer, L.I. Krishtalik, Electrostatic effects on electron-transfer kinetics in the cytochrome *f*–plastocyanin complex, Biophys. J. 73 (1997) 3265–3276.
[58] H.X. Zhou, Effects of mutations and complex formation on the reduction potentials of cytochrome c and cytochrome c peroxidase, J. Am. Chem. Soc. 116 (1994) 10362–10378.
[59] Yu.I. Kharkats, J. Ulstrup, Dielectric image effects in environmental reorganization free-energies and interreactant work terms of metalloprotein electron-transfer reactions, Chem. Phys. 141 (1990) 117–129.
[60] Y.-P. Liu, M.D. Newton, Reorganization energy for electron-transfer at film-modified electrode surfaces—a dielectric continuum model, J. Phys. Chem. 98 (1994) 7162–7169.
[61] ChemCraft, tool for treatment of the chemical data; http://www.chemcraftprog.com.

[62] G. Palmer, W.R. Dunham, J.A. Fee, R.H. Sands, T. Iizuka, T. Yonetani, The magnetic susceptibility of spinach ferredoxin from 77–250 degrees K: measurement of antiferromagnetic coupling between two iron atoms, Biochim. Biophys. Acta 245 (1971) 201–207.
[63] W.O. Gillum, R.B. Frankel, S. Foner, R.H. Holm, Synthetic analogs of the active sites of iron–sulfur proteins, XIII. Further electronic and structural relationships between the analogues $[Fe_2S_2(SR)_4]^{2+}$ and the active sites of oxidized 2Fe–2S proteins, Inorg. Chem. 15 (1976) 1095–1100.
[64] R.E. Anderson, W.R. Dunham, R.H. Sands, A.J. Bearben, H.L. Crespi, Nature of iron sulfur cluster in a deuterated algal ferredoxin, Biochim. Biophys. Acta 408 (1975) 306–318.
[65] L. Petersson, R. Cammack, K.K. Rao, Anti-ferromagnetic exchange interaction in the 2-iron–2-sulfur ferredoxin from the blue-green-alga spirulina-maxima studied with a highly sensitive magnetic balance, Biochim. Biophys. Acta 622 (1980) 18–24.
[66] E.A. Kanevskii, On the theory of electrode potential. I. The nature of the electrode potential and the problem of the possibility of calculation of the absolute electrode potential, Zh. Fiz. Khim. 22 (1948) 1397–1404.
[67] E.A. Kanevskii, It is possible to develop the thermodynamic theory of electrode potential? Zh. Fiz. Khim. 24 (1950) 1511–1514.
[68] E.A. Kanevskii, On the theory of electrode potential. III. Calculation of free energies of electrode processes and thermodynamic electrode potentials, Zh. Fiz. Khim. 26 (1952) 633–641.
[69] V.A. Pleskov, B.V. Ershler, On the calculation of single electrode potentials from spectroscopic and thermodynamic data, Zh. Fiz. Khim. 23 (1949) 101–103.
[70] B.V. Ershler, V.A. Pleskov, On the E.A. Kanevskii's "absolute" scale of electrode potentials, Zh. Fiz. Khim. 25 (1951) 1258–1260.
[71] H. Reiss, A. Heller, The absolute potential of the standard hydrogen electrode—a new estimate, J. Phys. Chem. 89 (1985) 4207–4213.
[72] Yu.V. Pleskov, The absolute potential of a standard hydrogen electrode—a new estimate—comment, J. Phys. Chem. 91 (1987) 1691–1692.
[73] S. Trasatti, The concept of absolute electrode potential. An attempt at a calculation, J. Electroanal. Chem. 52 (1974) 313–329.
[74] S. Trasatti, Relative and absolute electrochemical quantities—components of potential difference across electrode–solution interface, J. Chem. Soc. Faraday Trans. Part I 70 (1974) 1752–1768.
[75] A. Frumkin, B. Damaskin, Remark on the paper of S. Trasatti: the concept of absolute electrode potential. An attempt at a calculation, J. Electroanal. Chem. 66 (1975) 150–154.
[76] L.I. Krishtalik, The surface potential of solvent and the intraphase pre-existing potential, Russ. J. Electrochem. 44 (2008) 43–49.
[77] L.I. Krishtalik, Solvation energy of metallocenes pilot ions: beyond the Born approximation, Electrochim. Acta 53 (2008) 3722–3733.Corrigendum, ibid 54 (2009) 4741.
[78] S. Trasatti, Interfacial behaviour of non-aqueous solvents, Electrochim. Acta 32 (1987) 843–850.
[79] M.K. Gilson, B.H. Honig, The dielectric permittivity of a folded protein, Biopolymers 25 (1986) 2097–2119.
[80] H. Nakamura, T. Sakamoto, A. Wada, A theoretical-study of the dielectric-constant of protein, Protein Eng. 2 (1988) 177–181.
[81] T. Simonson, D. Perahia, G. Bricogne, Intramolecular dielectric screening in proteins, J. Mol. Biol. 218 (1991) 859–886.
[82] T. Simonson, D. Perahia, A.T. Brünger, Microscopic theory of the dielectric-properties of proteins, Biophys. J. 59 (1991) 670–690.
[83] G. King, F.S. Lee, A. Warshel, Microscopic simulations of macroscopic dielectric-constants of solvated proteins, J. Chem. Phys. 95 (1991) 4366–4377.
[84] P.E. Smith, R.M. Brunne, A.E. Mark, W.F. van Gunsteren, Dielectric-properties of trypsin-inhibitor and lysozyme calculated from molecular-dynamics simulations, J. Phys. Chem. 97 (1993) 2009–2014.
[85] T. Simonson, D. Perahia, Microscopic dielectric-properties of cytochrome-c from molecular-dynamics simulations in aqueous-solution, J. Am. Chem. Soc. 117 (1995) 7987–8000.
[86] E.L. Mertz, L.I. Krishtalik, Low dielectric response in enzyme active site, Proc. Natl. Acad. Sci. U. S. A. 97 (2000) 2081–2086.
[87] Y. Zu, M.M.-J. Couture, D.R.J. Kolling, A.R. Crofts, L.D. Eltis, J.A. Fee, J. Hirst, Reduction potentials of Rieske clusters: importance of the coupling between oxidation state and histidine protonation state, Biochemistry 42 (2003) 12400–12408.
[88] Y. Zu, S. Di Bernardo, T. Yagi, J. Hirst, Redox properties of the [2Fe–2S] center in the 24 kDa (NQO2) subunit of NADH:ubiquinone oxidoreductase (complex I), Biochemistry 41 (2002) 10056–10069.
[89] N.B. Ugulava, A.R. Crofts, CD-monitored redox titration of the Rieske Fe–S protein of Rhodobacter sphaeroides: pH dependence of the midpoint potential in isolated bc1 complex and in membranes, FEBS Lett. 440 (1998) 409–413.
[90] M. Guergova-Kuras, R. Kuras, N. Ugulava, I. Hadad, A.R. Crofts, Specific mutagenesis of the Rieske iron–sulfur protein in *Rhodobacter sphaeroides* shows that both the thermodynamic gradient and the pK of the oxidized form determine the rate of quinol oxidation by the *bc*1 complex, Biochemistry 39 (2000) 7436–7444.
[91] T. Simonson, G. Archontis, M. Karplus, A Poisson–Boltzmann study of charge insertion in an enzyme active site: the effect of dielectric relaxation, J. Phys. Chem. B 103 (1999) 6142–6156.